J. Mt. Sci. (2011) 8: 390-402
DOI: 10.1007/s11629-011-2064-0

Digital Terrain Modelling Using Corona and ALOS PRISM Data to Investigate the Distal Part of Imja Glacier, Khumbu Himal, Nepal

LAMSAL Damodar*[1], SAWAGAKI Takanobu[2] and WATANABE Teiji[2]

1 Graduate School of Environmental Science, Hokkaido University, N10, W5, Sapporo, 060-0810, Japan

2 Faculty of Environmental Earth Science, Hokkaido University, N10, W5, Sapporo, 060-0810, Japan

** Corresponding author, e-mail: lamsal@wwwgeo.ees.hokudai.ac.jp; Phone: +81-11-706-2275*

Abstract: This study used Corona KH-4A and Advanced Land Observing Satellite (ALOS) PRISM images to generate digital terrain models (DTMs) of the distal part of Imja Glacier, where a few supra-glacial ponds (~0.07 km²) expanded into the large Imja Glacier Lake (Imja Tsho, ~0.91 km²) between 1964 and 2006. DTMs and subsequently derived topographical maps with contour intervals of 1 m were created from the high-resolution images (Corona in 1964 and ALOS in 2006) in the Leica Photogrammetric Suite (LPS) platform. The DTMs and topographic maps provided excellent representation of the elevation and micro-topography of the glacier surface, such as its supra-glacial ponds/lake, surface depressions, and moraine ridges, with an error of about +/- 4 m (maximum). The DTMs produced from the Corona and ALOS PRISM images are suitable for use in studies of the surface change of glaciers. The topographical maps produced from the Corona data (1964) showed that part of the dead ice in the down-glacier area was even higher than the top of the lateral moraine ridges, while the glacier surface in the up-glacier area was noticeably lower than the moraine crests. This suggests more extensive melting of glacier ice in the up-glacier area before 1964. The average lowering of the glacier surface from 1964 to 2006 was 16.9 m for the dead-ice area west of the lake and 47.4 m for the glacier surface east of the lake; between 1964 and 2002, the lake surface lowered by 82.3 m. These figures represent average lowering rates of 0.4, 1.1, and 2.2 m/year for the respective areas.

Keywords: Imja Glacier; Nepal Himalaya; DTM; Topographic map; Surface lowering; Corona; ALOS PRISM

Received: 28 September 2010
Accepted: 30 March 2011

Introduction

Many debris-covered valley glaciers in the Nepal Himalaya have been losing mass due to climate warming (Benn et al. 200l; Bolch et al. 2008a). Shrinkage and morphological changes in debris-covered glaciers have been detected by repeated field observation and from examination of multi-temporal stereo-pair images/photographs that cover a considerable time span (Iwata et al. 2000). Down-wasting dominants over the horizontal retreat of debris-covered glaciers, and changes in such glaciers are largely recognizable through the lowering of their surface (Kadota et al. 2000; Bolch et al. 2008a). About one-third of the large valley glaciers in Khumbu Himal are debris-covered (Fujii and Higuchi 1977), some of the largest being Ngozumpa, Khumbu, Lhotse and Imja glaciers.

Supra-glacial ponds/lakes are likely to form on

the surface of these debris-covered glaciers when conditions are favourable (Reynolds 2000): glacier surface gradient less than 2°; low ice velocity or complete stagnation. Benn et al. (2001) carried out intensive field observations and took measurements of the supra-glacial lakes of the Ngozumpa Glacier to characterize their growth mechanism and identify the factors that control their growth. Studying and monitoring debris-covered glaciers are important from the perspective of hazards because glacial lakes sometimes produce devastating glacial lake outburst floods (GLOFs) (Quincey et al. 2007).

The Imja Glacier is one of the most extensively researched glaciers in the Himalaya (e.g., Hammond 1988; Watanabe et al. 1994; Sakai et al. 2007; Bolch et al. 2008b; Hambrey et al. 2008). Most studies have focused primarily on lake development (e.g., Bajracharya et al. 2007a; Byers 2007), the expansion characteristics of Imja Glacier Lake (hereafter referred to as Imja Tsho) (e.g., Yamada 1998; Watanabe et al. 2009; Ives et al. 2010), and the associated hazards of GLOFs (e.g., Bajracharya et al. 2007b). Watanabe et al. (1995) and Fujita et al. (2009) discussed ice melting that caused surface lowering in the dead-ice area of the Imja Tsho based on ground measurements for the shorter period between 1984 and 1989 and between 2001 and 2007, respectively. However, our knowledge of the vertical lowering of the glacier surface in the immediate vicinity of the lake (dead-ice and active glacier) over a longer period is minimal.

Stereo-capable data from different times are required in order to calculate volumetric changes of debris-covered glaciers because non-stereo data, such as multispectral Landsat images cannot be used to produce three-dimensional (3D) topographical maps. Multi-temporal high-resolution stereo-data can expand our understanding of the morphological changes of a glacier surface.

The Advanced Land Observing Satellite (ALOS), launched in 2006, has three sensors: PRISM, ANVIR, and PALSAR. Among these, ALOS PRISM has a stereo capability that can generate DTMs and 3D maps. There have been few studies that have investigated planimetric changes in glaciers in the Himalaya using ALOS data (e.g., Ye et al. 2009). Corona data, on the other hand, has a complex geometry, lacks metadata (ephemeris) pertaining to image acquisition, and requires highly sophisticated image-processing software to extract 3D information. However, Corona data provides an invaluable resource for investigation in various fields such as glaciology and archaeology.

The combined use of ALOS PRISM and Corona stereo-data to produce DTMs and topographical maps of a Himalayan glacier has not been attempted hitherto. The first objective of this paper, therefore, is to present a methodology for producing accurate DTMs and detailed topographical maps from stereo-pair data (Corona and ALOS). The second objective is to use these results to demonstrate the changes that occurred in and around Imja Tsho in the distal part of the debris-covered area of the Imja Glacier for the 42 years from 1964 to 2006. This is the period that has witnessed the development of Imja Tsho (Watanabe et al. 2009).

The Imja Glacier (27° 54' N and 86° 56' E) is located in Sagarmatha (Mt. Everest) National Park in eastern Nepal (Figure 1a). It converges with Lhotse Shar Glacier from the north to form a single glacier taking the name of Imja Glacier. Ambulapche Glacier from the south merges with it, but has become increasingly isolated from Imja Glacier due to stagnation and retreat. Imja Tsho has formed on the distal part of the lower Imja Glacier. In the current study, the distal part (study area) refers to a section of the glacier between the terminus and the point where the two glaciers converge. This covers an area about 3.65 km^2, including Imja Tsho and glacier (~2.50 km^2), together with the immediate surroundings (~1.15 km^2). Five small supra-glacial ponds initiated the formation of the lake in the 1950s. They expanded and coalesced to form a large lake by the 1970s (Hammond 1988; Watanabe et al. 2009). The dimensions of the lake in 2007 were ~2000 m in length, ~650 m in width, and ~1.03 km^2 in area (Watanabe et al. 2009). By 2002, the lake had an average depth of 41.6 m and a maximum depth of 90.5 m (Sakai et al. 2003). The northern and southern shorelines had expanded so that by 1984 they were in contact with the lateral moraines (Watanabe et al. 2009). The western shoreline rested against the lower dead-ice area and the eastern shoreline was under-cutting the debris-covered ice cliffs of the glacier front (Figure 1b).

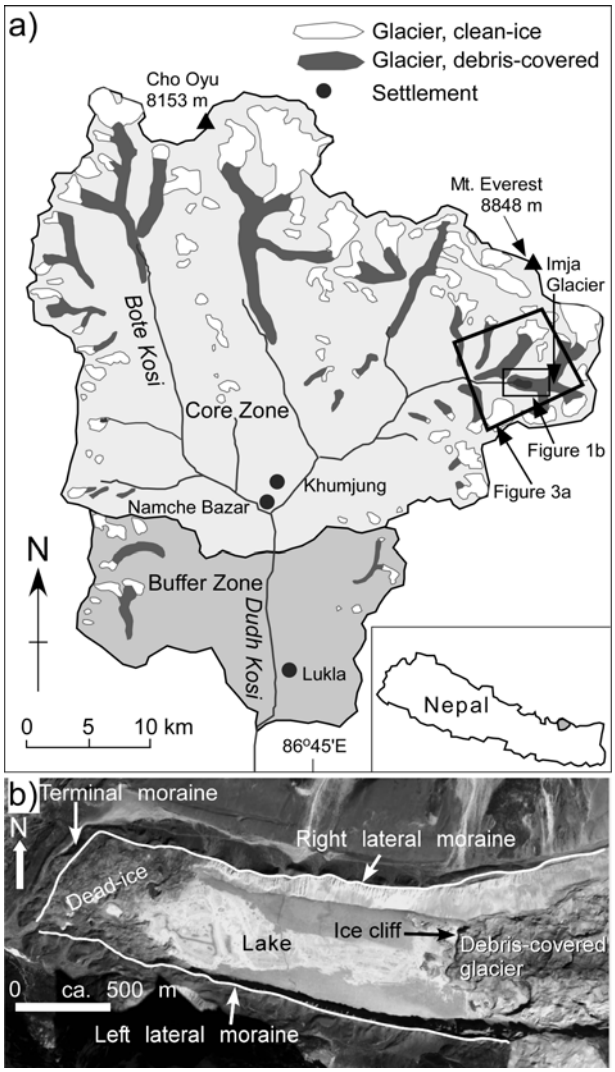

Figure 1 Location of the Imja Glacier (a) and landform features around Imja Tsho (b)

1 Data Utilized

1.1 ALOS PRISM data

ALOS PRISM acquires data in triple mode to generate an accurate Digital Surface Model and < 10 m geometric accuracy is achievable (Tadono et al. 2009). According to the Remote Sensing Technology Centre of Japan (RESTEC), RMSE of ALOS PRISM RPC in the range of 0.5 to 10 m; however, in most cases, the errors are in the range of 1 to 5 m (http://www.alos-restec.jp/products_e.html). The accuracy of the data/results presented in this paper relies largely on the quality of the stereo-model generated from ALOS stereo-data with RPC.

ALOS PRISM data (dated 4 December 2006; spatial resolution, 2.5 m) in triple mode F, N, and B (forward, nadir, and backward) with processing level 1B1 (radiometrically calibrated data) plus RPC data file were obtained from the RESTEC. Details of the data used in this study are listed in Table 1.

Table 1 Parameters of Corona and ALOS data used in this study

Sensor	ALOS PRISM	Corona
System	Stereo-Triple (F, N and B)	KH-4A, stereo (F and B)
Camera /sensor type		Panoramic, panchromatic
Date of acquisition	04/Dec./2006	26/Nov./1964
Film resolution		120 lines pair/mm
Focal length		24 inches (609.6 mm)
Ground coverage	35 × 35 km	17 × 232 km
Ground resolution	2.5 m	2.7–7.6 m
Flight height	691.65 km	185 km
Image scale		1: 305,000

1.2 Corona data

Images acquired from Corona camera systems KH-1, KH-2, KH-3, KH-4, KH-4A, and KH-4B were declassified in 1995 and became available in a digital format in 2003 (McDonald 1995; Galiatsatos et al. 2008). The early systems of KH-1, KH-2, and KH-3 were equipped with a single panoramic camera, while the latter systems of KH-4, KH-4A, and KH-4B were equipped with both forward- and backward-looking cameras. The images taken by the KH-4, KH-4A, and KH-4B camera systems, which have a stereo capability, a higher spatial resolution (3.00 - 7.60, 2.70 - 7.60 and 1.8 - 7.60 m, respectively) and wide area coverage offer the oldest available stereo data. Corona images have been discussed extensively by Dashora et al. (2007) and Galiatsatos et al. (2008).

Geometric distortions inherent in filmstrips from a panoramic camera need to be corrected to achieve precise results (Slama 1980, Figure 2a). Typical geometric distortions of a Corona image (Figure 2a) gradually increase from the centre (minimal distortion) to the extreme edges (maximal distortion) of an image along the track. The processing of Corona stereo images for DTM

generation has been well described (Altmaier and Kany 2002; Bolch et al.2008a; Casana and Cothren 2008).

Corona KH-4A stereo-pair images (dated 26 November 1964) of the Everest area were obtained from the USGS in a digital format scanned at 3600 dpi (7 microns). The image IDs are DS1014-2118DF192 (forward-looking) and DS1014-2118DA194 (backward-looking). Of the total (17 × 232 km) ground coverage of Corona KH-4A images, only a small portion (5 × 8 km) was cropped from both the backward and forward images (as shown in a box in Figure 2b).

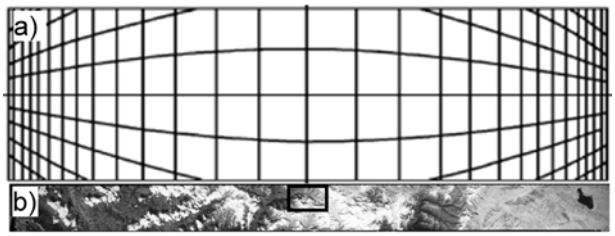

Figure 2 Typical film distortion by Corona panoramic camera (a) (Slama 1980), and footprint (17 × 232 km) of the Corona image used in this study (b). Only a forward image, DS1014-2118DA194, is shown here. The Imja Glacier area is enclosed in a box.

2 Development of Image and Data Processing Methodology

2.1 Image processing platform

To generate DTMs, stereo images were processed with the aid of Leica Photogrammetric Suite (LPS 9.3) in the ERDAS IMAGINE workstation. Topographic maps and Digital Elevation Models (DEMs) were produced from the DTMs after the rigorous editing of the triangulated irregular network (TIN) model (vector DTM). DEMs and topographic maps were later used for analytic and interpretative purposes in the ESRI ArcGIS platform.

The use of LPS 9.3 with PLANAR SD 2020 Stereo Mirror™/3D Monitor and Leica 3D TopoMouse facilitates and enhances stereo viewing, GCP collection for Corona data (Figure 3a), and terrain editing.

LPS 9.3 has the capability to represent a terrain (DTM) either in vector or in raster format. The elevation of a raster DTM is not editable, but Leica Terrain Format (LTF), a TIN model, is fully editable. This is important because automatically generated DTM contains numerous errors, such as false spikes and depressions, which lead to an inaccurate terrain representation. These errors most probably occurred due to irregular micro-topography, high relief and shadow on the images. Therefore, LTF was used so that editing was possible to generate an accurate terrain model. A TIN can be edited as mass points or nodes of TINs, break lines, and contour lines that are perceptible in 3D viewing, and terrain representation can take the form of mass points, triangles, and contour lines (Figure 3b).

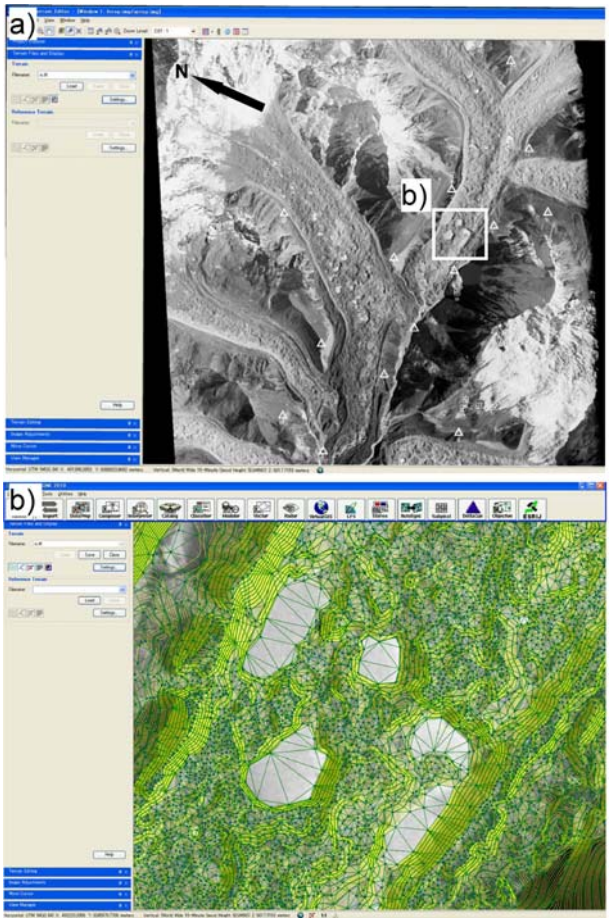

Figure 3 Location of ground control points (GCPs) denoted by white triangles (a) and representation of landform by mass points, triangles, and contour lines in vector DTM (LTF) (b). The white box in Figure 3a shows the area of Figure 3b.

2.2 Data processing

2.2.1 ALOS PRISM

ALOS PRISM images with a Rational Polynomial Coefficient (RPC) file, which contains

the interior and exterior information necessary to perform aerial triangulation, were processed first. RPC file, whose datum is geoid height, alone, is sufficient for triangulating the stereo-images. However, input of one or more GCPs enhances the accuracy of DTM. ALOS PRISM images (F, N, and B) with RPC file and three GCPs (collected from the NGS map, Everest area 1988) were employed to triangulate (RMSE ~0.40) stereo-images to create a stereo model and were used for DTM generation. A stereo-model was generated for the entire area covered by the scenes; however, DTM of the study area only was created.

Because the data from both ALOS and Corona have a high spatial resolution and are processed upon viewing the stereo-model, accurate placement and editing of the mass points on the terrain surface were possible. Accurate placement refers to the 3D cursor/mass point just exactly touching the terrain surface. The vector DTM was edited upon viewing the stereo-model as a base, where the 2D mouse cursor behaves as a 3D cursor. Whenever the 3D cursor touched on the terrain surface, a mass point was registered manually with 3D cursor click. A mass point is a node of TIN on the terrain surface that has X, Y, and Z (longitude, latitude, and altitude) values in metres and is the primary form of terrain representation and editing. The number of mass points required to represent a particular geographic feature such as a ridge and depression on the terrain surface depends largely on regularity or uniformity and size of the feature, spatial resolution of image data, and desired accuracy.

Terrain representation in areas of shadow, irregular micro-landform, high relief, and at the margins of the produced DTM contained numerous errors that called for much terrain editing. The floating or sinking of a mass point produces so-called 'bad points' that were carefully removed manually or interactively using LPS 9.3 Terrain Editor, which has various embedded functions or filters that remove such errors. Extensive editing was carried out upon viewing the stereo-model as a base until satisfactory terrain representation was achieved. Thick or thin distribution of mass points that did not duly represent ridges, ponds, and depressions were also edited to ensure that enough mass points had truly represented the landforms. Most frequently employed densification and rarely applied thinning,of mass points was carried out during terrain editing, so that the produced DTM would represent the actual terrain surface. Editing involved densification, thinning, and placement of masspoints on the terrain that lay above or beneath the terrain surface. After editing, a highly satisfactory DTM was produced. The DTM editing processes for ALOS described here were also applied to the Corona data (see below).

2.2.2 Corona

Photogrammetric software requires interior and exterior orientation parameters (IOPs and EOPs) to correct geometric distortions. IOPs that include the camera model and image parameters (mainly 'fiducial marks' and 'principal point') together with EOPs (GCPs) are generally used to remove these geometric distortions and to perform aerial triangulation (Altmaier and Kany 2002). However, 'fiducial marks' and 'principal point' do not exist in Corona images.

To correct the geometric distortions of the Corona images, we employed a non-metric camera model in the LPS 9.3 platform. This requires only the focal length, pixel size of the scanned image, and flying height of the camera platform as input for IOPs (Altmaier and Kany 2002; Casana and Cothren 2008). LPS automatically sets the principal point at the image centre or as a zero value, and it treats a part of an image as an entire filmstrip (Altmaier and Kany 2002). The remaining process is similar to that used for an image taken by a frame camera that has 'fiducial marks' and 'principal point'.

Acquiring reliable ground control points (GCPs) from identical locations is one of the most crucial tasks in the production of accurate DTMs and topographical maps. This task largely determines the quality of the final products. The source of GCPs for the Corona was one of the image data used in the study itself (ALOS PRISM), which reduced the possibility of mis-targeting. Such mis-targeting is likely when one uses topographic maps as the source of GCPs. The collected GCPs were taken from unchanged sites outside the moraines based on careful observation. Objects identifiable in the ALOS images were also identifiable in the Corona images. Moreover, several field campaigns and ground photographs taken during the

fieldwork greatly facilitated the identification of objects and landforms on the images.

A large number of GCPs, and their even distribution and accuracy, are important factors that determine the quality of triangulation and the DTM produced (Altmaier and Kany 2002; Galiatsatos et al. 2008; Bitelli and Girelli 2009). The GCPs for the Corona images were taken from a corrected ALOS-scene (ALOS stereo-model), with meticulous care given to their accuracy and even distribution. In this manner, the Imja Glacier and its immediate area was surrounded by the 15 GCPs (whose locations can be seen in Figure 2a). Afterwards, some 80 tie points were automatically generated with image matching technique on stereo-data based on the provided IOPs and EOPs. All the tie points were automatically placed at the correct locations on both images (forward and backward). Aerial triangulation was then performed (RMSE ~0.70 pixel) to produce a vector DTM or TIN. RMSE error of the aerial triangulation for Corona was small because of the small subset of data used, high spatial resolution of the data and enhanced stereo viewing with the PLANAR StereoMirror/3D Monitor for collecting and placing GCPs.

3 Results

3.1 Evaluation of the accuracy of the produced DTMs

As shown in Figure 1b, the Imja Glacier is surrounded by lateral and terminal moraines. The glacier surface within the lateral and terminal moraines is subject to surface changes (lowering) due to glacier melt. It is assumed that the surface beyond the lateral moraines has remained unchanged (i.e., elevation change through time should be negligible or zero – small changes of tens of centimetres to a metre are considered insignificant). This unchanged surface (buffer of ~1.15 km^2) beyond the lateral moraines is used for assessing the accuracy of the produced DTMs and the topographical maps.

Figure 4a is a portion of the elevation change map outside the lateral moraines (unchanged ground) of the Imja Glacier. The glacier surface area within the lateral moraines was masked for the calculation. The difference between the Corona and ALOS DTM ranges from 4 to -3 m (Figure 4a).

To quantify the dominance of error, a histogram of DEM differences was prepared (Figure 4b). The calculations were performed on a 2 × 2 m grid, and the total pixel count was 281339. Later, the pixel count for each class was converted to error percentage. The class with the most dominant DTM difference was -1–0 m (31%) while the least influential class was 3–4 m (1.5%). The range of DEM difference from -2 to 2 m accounts for 86.5% (overwhelming dominance), and the range from -1 to 1 m comprises 53.5% (majority dominance). We concluded that a maximum relative DEM error of 4 m may exist in the generated DTMs and topographic maps in this study.

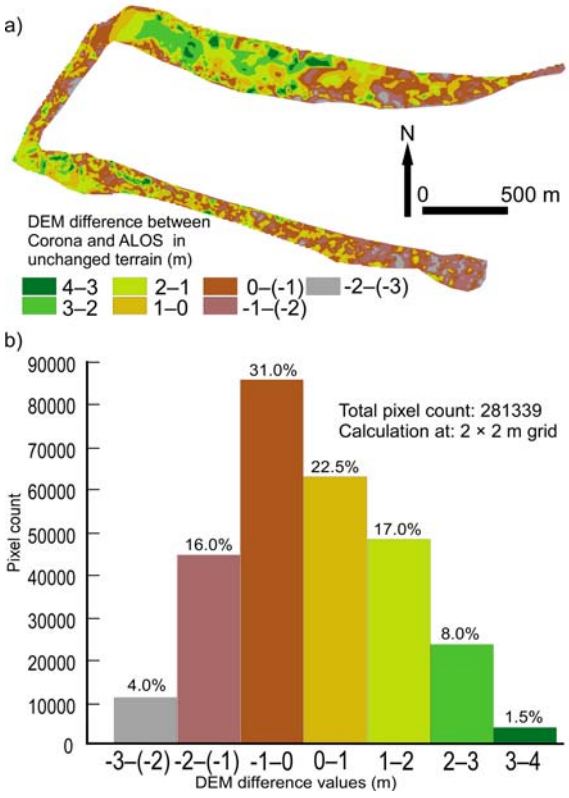

Figure 4 Portion of the elevation change map beyond the lateral and terminal moraines, showing unchanged areas (a), and a histogram of DEM differences (b).

3.2 DTM and topographic maps by Corona and ALOS PRISM

A view of a topographic representation as a DTM formed by mass points, triangles, and contour lines is shown in Figure 2b. The TIN DTM

after extensive editing has well represented the micro-landforms such as the small ponds, depressions, and moraine ridges (Figure 2b).

Figure 5a shows the topography around Imja Tsho in 1964 at contour intervals of 1 m (faint lines), 10 m (lighter bold lines), and 20 m (bold lines) as mapped by Corona stereo images. Figure 5b shows the topography in 2006 as mapped by ALOS PRISM images. DEMs for 1964 (Figure 6a) and 2006 (Figure 6b) around the lake were generated from vector DTMs of these respective years. The topographies for both years are represented in 11 classes (ranging from 4960–4980 to 5160–5180 m).

The water level of Imja Tsho was 5006 m in 2006 (Figure 5b). Watanabe et al. (2009) reported that the level was 5004 m in 2006, based on the field measurements. This 2 m difference falls within the DEM error (maximum: 4 m). It should be noted that Fujita et al. (2009) suggested there were no significant changes in the lake level between 2001 and 2007[1)].

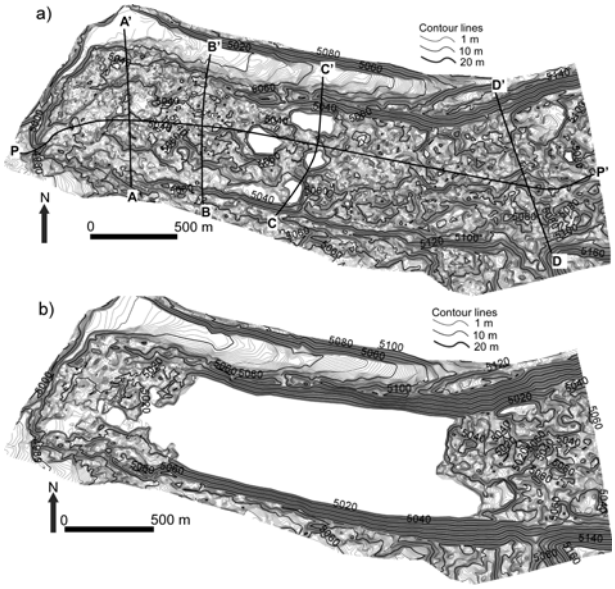

Figure 5 Topographic maps around Imja Tsho in 1964 (a) and 2006 (b). Contour intervals: 1 m (faint lines), 10 m (lighter bold lines), and 20 m (bold lines).

This study also produced accurate measurements for the area of the supra-glacial ponds that existed in 1964: 0.021, 0.019, 0.008, 0.008 and 0.012 km² (total area: 0.068 km²), and of the lake in 2006: 0.913 km². The pond/lake boundary was delineated from the surrounding moraines/glacier upon viewing the DTM superimposed over the stereo-model of ALOS PRISM. The surroundings are higher than the lake surface, and texture of the lake is also different from them; so the flat lake surface is easily identifiable on the stereo-model. Uncertainty in delineating the precise lake boundary over the stereo-model is believed to be very small: less than a meter.

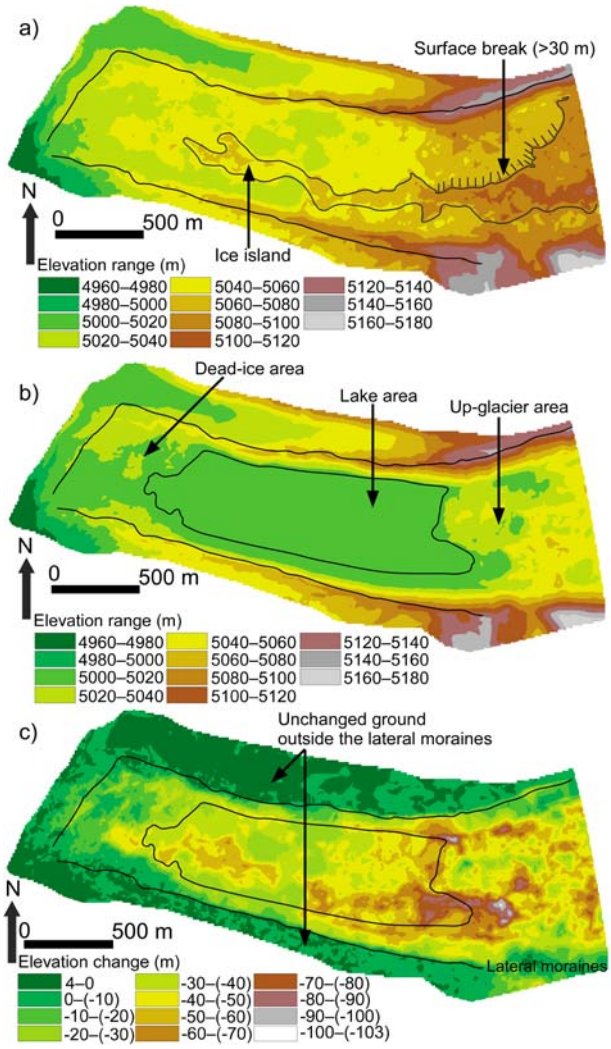

Figure 6 Digital Elevation Model (DEM) of the Imja Glacier in 1964 (a), DEM for 2006 (b), and elevation change map showing the lowering of the glacier surface over the four decades from 1964 to 2006 (c).

1) Our field survey conducted in November 2009 also shows that no lake level change occurred between 2006 and 2009.Watanabe et al. (2009) described in the left column of page 263, lines 23–25, "They [Mool et al. 2001] misleadingly suggested that the level of Imja Tsho has been rising and consequently, classified it as dangerous". However, this depiction was mistaken and should be omitted.

3.3 Glacier surface lowering from 1964 to 2006

The topographical maps (Figure 5) and DEMs (Figure 6) clearly show that the elevations of the debris-covered glacier surface have changed extensively. The map of elevation change for the entire area (Figure 6c) was produced by subtracting the DEM values for 2006 (Figure 6b) from those for 1964 (Figure 6a). The values for elevation change are presented in 12 classes (Figure 6c). Extensive surface lowering that is as high as 102.3 m is visible in the up-glacier area. An elongated higher surface extends parallel to the glacier direction (east to west) in the 1964 DEM, as shown in Figure 6a. Such a relatively high ice ridge is defined as an 'ice island', and an ice cliff higher than 30 m is defined as a 'surface break' in this study. A 'surface break' might have separated the dead-ice area from the active glacier although further studies are needed for confirmation.

The average lowering of the glacier surface (calculated for 2 × 2 m grids using the elevation change map, Figure 6c) for the 42 years from 1964 to 2006 in the dead-ice area west of the lakeshore is 16.9 m. The average lowering in the up-glacier area east of the lakeshore is 47.4 m. These calculations give lowering rates of 0.4 and 1.1 m/year for the respective areas.

The surface lowering in the lake area in 2006 shown in Figure 6c is based on the 2006 lake water level (5006 m). However, the bottom of the lake is a better benchmark for the calculation of glacier melting although no data on the lake bottom depths are available for 2006. This study, therefore, employed a 2002 bathymetric map prepared by Sakai et al. (2003). Figures 7a and 7c show a bathymetric map of the lake for 2002 and a topographic map for 1964 that covers the same area. These maps (Figures 7a and 7c) were converted to DEMs, as shown in Figures 7b and 7d. The elevation change map in the lake area of 2002 (Figure 7e) was produced by subtracting the 2002 lake bottom values (bathymetric DEM) from the

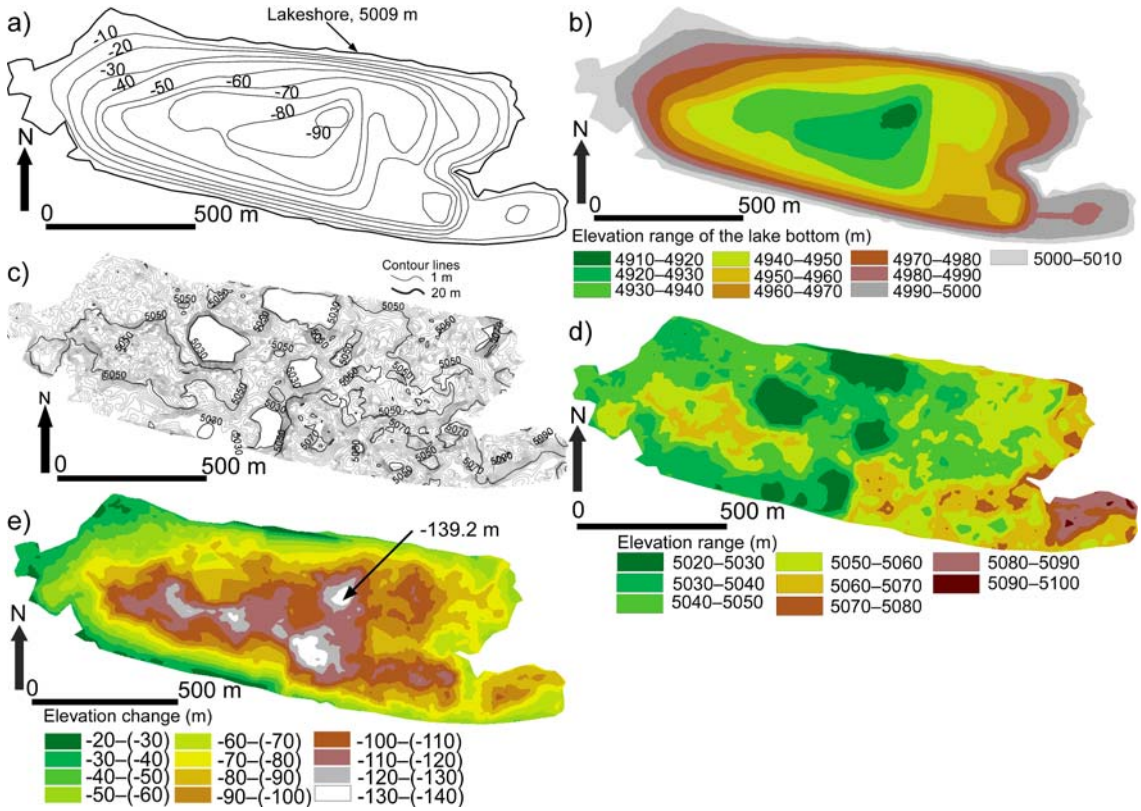

Figure 7 Bathymetric map of Imja Tsho in 2002 reproduced from Sakai et al. (2003) (a), DEM of the lake bathymetry derived from Figure 7a (b), topographic map of the 1964 glacier surface in the same area as that of the 2002 lake (c), DEM of the 1964 glacier surface derived from Figure 7c (d), and elevation change map (e). The surface lowering from the glacier surface in 1964 to the lake bottom in 2002 can be seen in the elevation change map.

1964 glacier surface values (DEM). The average surface lowering for the 38 years from the 1964 glacier surface to the 2002 lake bottom (Figure 7e) was 82.3 m at a rate of 2.2 m/year, and the maximum surface lowering during this period was 139.2 m (Figure 7e).

Cross-sectional profiles across the glacier/lake and a longitudinal profile along the glacier surface (Figure 8) were created in order to gain better insight into the changes on the glacier surface. The profiles were based on the topographical maps of 1964 and 2006, and the bathymetric map of the lake in 2002 (Sakai et al. 2003). Profile A–A' in the dead-ice area reveals that some parts of the glacier surface (e.g. an 'ice island') were higher than the top of the lateral moraines in 1964.

The maximum surface lowering from 1964 to 2006 at the 'ice island' (A–A' in Figure 8) was 51 m

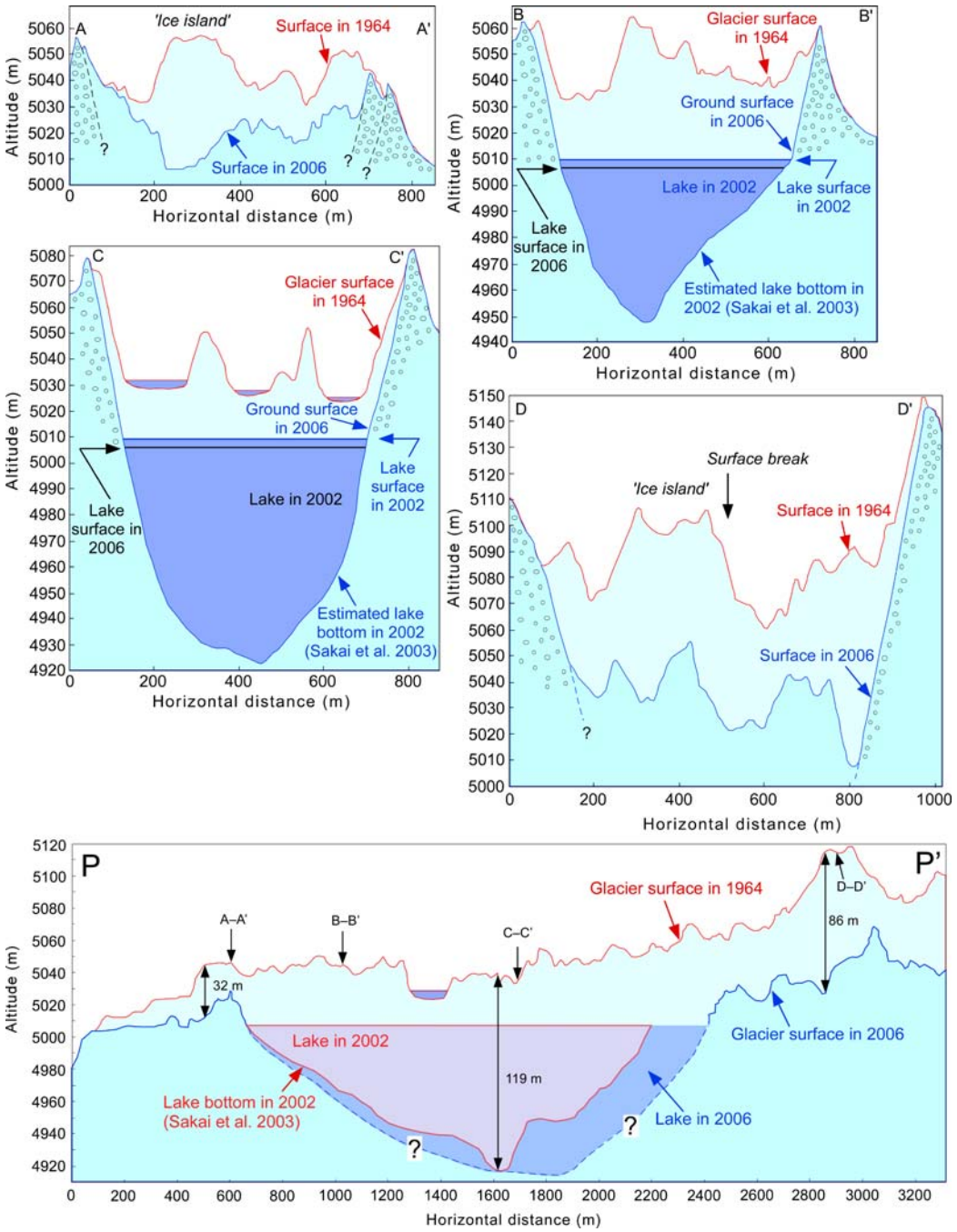

Figure 8 Cross sections (A–A', B–B', C–C', D–D') and longitudinal section (P–P') showing the glacier topography. The glacier lake bottom and lake surface for 2002 were taken from Sakai et al. (2003). For the locations of the profiles, see Figure 5a.

(5057–5006 m). Profile D–D' in the up-glacier area shows a greater surface lowering (a maximum of 84 m, from 5092 m to 5008 m). Profiles B–B' and C–C' across the glacier/lake show greater surface lowering (a maximum of 114 m, from 5065 m to 4951 m in B–B', and 120 m, from 5050 m to 4930 m in C–C') during the 38 years between 1964 and 2002.

Longitudinal profile P–P' shows the extent of the surface lowering along the up-glacier area, the lake area, and the dead-ice area. Along profile P–P' (Figure 8), the maximum surface lowering in the dead-ice area and up-glacier area for the 42 years from 1964 to 2006 was 32 m (from 5044 m to 5012 m) and 86 m (from 5114 m to 5028 m), respectively, while the maximum surface lowering in the lake area for the 38 years from 1964 to 2002 was 119 m (from 5038 m to 4919 m).

4 Discussion

4.1 DTM generation and accuracy evaluation

As stated above, previous use of Corona data to generate a DTM has been extremely limited. Altmaier and Kany (2002) authored one of the earliest studies that employed Corona KH-4B products to generate DSM in Morocco. Bolch et al. (2008a) deployed Corona (KH-4) and ASTER (spatial resolution, 15 m) DTMs to explore the suitability of these data for the detection of volumetric glacier changes in Mt. Everest area. To produce accurate DTMs in the present study, we employed a combination of Corona (KH-4A) and ALOS PRISM data.

Our first attempt in generating DTM with automatic procedures was largely unsatisfactory. Major errors were caused by the poor representation of terrain by bad mass points resulting to false spikes and depressions: a few metres to hundreds metres up (on the air) or below the terrain surface, and to too thick or thin distribution of mass points. This prompted extensive editing to remove unnecessarily thick mass points, and to add mass points where their distribution was thin. Low contrast and dark shadows in the images were problematic in the placement of mass points on the terrain surface. Despite the fact that we, (1) took great care with the collection of GCPs, (2) employed high-resolution stereo-image data, (3) performed extensive editing of DTMs, and (4) deployed highly sophisticated photogrammetric software (LPS 9.3), there could still be small errors (maximum: 4 m) in the DTMs and topographical maps. However, representation of the terrain of the glacier surface was entirely satisfactory for the present purpose. Good DTMs (4 m maximum error) is achievable with the data and methods presented here especially in gentle/moderate topography; however, the error could be larger in high relief mountains as such events are witnessed (e.g., Bolch et al. 2008a).

Toutin (2002), who gave a detailed description of the generation and editing of raster DEM using ASTER (spatial resolution, 15 m) stereo-data with the aid of PCI Geomatics OrthoEngine 7.0, also mentioned the difficulty he encountered in detecting the surface of featureless flat bodies such as a lake surface. However, in LPS 9.3, editing can be done manually with vector DTM (LTF) in a 3D viewing environment. Moreover, we can perceive the elevation of the surface with the aid of a 3D floating cursor so that the surface level of a flat body, such as a lake, can be detected. As a result, a lake surface and its absolute altitude can be determined. As stated before, automatically generated DTM could not delineate the lake boundary well. Therefore, manual editing was needed; all the bad points within the lake needed to be removed or corrected, and new mass points were placed along its boundary by viewing the stereo-model.

Fujita et al. (2008) suggested that remote-sensing DEMs based on ASTER and SRTM data are not applicable to monitoring altitudinal changes on moraine ridges. However, our study demonstrates that the use of high-resolution Corona and ALOS data in the LPS platform can produce sufficiently accurate DTMs and detailed topographical maps, thus overcoming the problems observed in previous studies.

4.2 Changes in surface topography

An 'ice island' on the glacier surface running from east to west, was identified (shown in Figure 6a), and the lower part of the 'ice island' had melted to form Imja Tsho, therefore, its area is

shown as a large negative elevation change (see Figures 6c and 7e).

The glacier surface in 1964 along profiles C–C' and D–D' was considerably lower than the top of the lateral moraines, in contrast with the down-glacier profiles (A–A' and B–B'). This suggests that by 1964, there had already been considerable glacier ice melting. In spite of the higher melting rate, in 1964 the up-glacier area had a steeper gradient. A noticeable topographic 'surface break' observed in the 1964 up-glacier area (Figures 5a and 6a) implies that the active glacier (up-glacier) had already separated from the dead ice. The gentler surface condition in the lower half of the mapped area (Figure 6) had already become conducive to the initiation of the small supra-glacial ponds before 1964.

Surface lowering in the dead-ice area of the Imja Glacier was examined for a shorter period, from 1989 to 1994 by Watanabe et al. (1995), and from 2001 to 2007 by Fujita et al. (2009). However, the surface lowering of the lake and the up-glacier areas had not been analyzed in the previous studies as stated earlier. The average lowering rate was calculated at 0.4 m/year for the dead-ice area west of the lake, 1.1 m/year for the up-glacier area east of the lake, and 2.2 m/year for the lake surface. The rate of surface lowering in the up-glacier area was approximately three times higher than that in the dead-ice area. Although studies of the dead-ice melting are important in terms of mitigating the danger of a GLOF in the case of Imja Tsho, we ascertained that the up-glacier area has been geomorphologically dynamic. Further, we found that the rate of surface lowering in the up-glacier area was half of that in the lake area. This difference, needless to say, is due to the effect of more rapid melting caused by water in contact with the glacier/ice body.

The central objective of this study is to present the morphological changes for the lake, and immediately down-glacier (dead-ice area) and up-glacier (active glacial area) of the distal section of the Imja Glacier between 1964 and 2006. There are no previous studies reporting morphological changes for glacial lakes for such a long period, for instance, between 1964 and 2002 (38 years) before and after the formation of a large lake. From this point of view, the study reported here is unique, and morphological changes for the lake may not be comparable to changes in other glaciers that do not have superimposed lakes. However, it will serve as a base study providing for discussion and comparison of morphological changes in the future development of glacial lakes elsewhere. Discussion of ice dynamics is largely beyond the scope of the present study on morphology; however, in the dead-ice area changes of the glacier (0.4 m/year) and the up-glacial section (1.1 m/year), in spite of covering only a small area, can be compared with previous studies in the region. Our results agree with those of Kadota et al. (2000) and Bolch et al. (2008a). Kadota et al. (2000) calculated a surface lowering rate of 0.6 – 0.8 m/year in 17 years (1978 to 1995) in the ablation area of the Khumbu Glacier, and Bolch et al. (2008a) also reported 0.5 – 1.2 m/year of surface lowering in 40 years from 1962 to 2002 for the same glacier. According to Quincey et al. (2007 and 2009), the researched distal part of Imja Glacier falls in low gradient (<2°) and stagnant or low glacial velocity zone, which favours for glacial melting. The higher surface lowering rate in the up-glacier area of Imja Glacier (1.1 m/year) over the dead-ice area (0.4 m/year) is probably due to thinner debris-cover in the up-glacier area as suggested in Khumb Glacier (e.g., Bolch et al. 2008a). This occurs because thick debris-cover suppresses ice/glacier melting (Benn et al. 2001).

5 Conclusions

This study used the images of Corona KH-4A (spatial resolution, 2.7–7.6 m) and ALOS PRISM (spatial resolution, 2.5 m) to generate DTMs with 2 m spatial resolution and subsequently derived topographical maps with contour intervals of 1 m. The high-resolution image data derived from Corona in 1964 and ALOS in 2006 in the LPS platform (particularly LTF vector DTM and its subsequent editing) produced sufficiently accurate DTMs and detailed topographical maps with a small margin of error (maximum: 4 m). These DTMs are suitable for the investigation of the surface changes of glaciers.

The topographical map derived from Corona DTM (1964) shows that part of the dead ice had been higher than the top of the lateral moraine ridge. The glacier surface in the studied area in

1964 along up-glacier profiles was considerably lower than the top of the lateral moraines, in contrast with the down-glacier profiles. This suggests that by 1964, there had already been a greater degree of glacier ice melting in the up-glacier area.

The average lowering of the glacier surface between 1964 and 2006 was 16.9 m for the dead-ice area west of the lake, and 47.4 m for the glacier surface east of the lake. The average lowering in the lake area between 1964 and 2002 was 82.3 m. This gives average lowering rates of 0.4, 1.1, and 2.2 m/year for the respective areas.

Acknowledgements

The authors would like to thank Jack D. Ives of Carleton University, Ottawa, Canada, and anonymous reviewers for improving this paper. The authors also like to thank Yamanokuchi T. (RESTEC) and Tadono T. (JAXA) for their valuable information for ALOS PRISM and Corona image processing. The authors are thankful to the Japan Science Society (Sasagawa Research Fund) and the Global Centre of Excellence (GCOE) programme by JSPS for partial funding to the first author.

References

Altmaier A, Kany C (2002) Digital surface model generation from CORONA satellite images. ISPRS Journal of Photogrammetry and Remote Sensing 56(4): 221–235.

Bajracharya SR, Mool PK, Shrestha BR (2007a) Impact of Climate Change on Himalayan Glaciers and Glacial Lakes: Case Studies on GLOF and Associated Hazards in Nepal and Bhutan. United Nations Environment Programme (UNEP).

Bajracharya B, Shrestha AB, Rajbhandari L (2007b) Glacial lake outburst floods in the Sagartmatha regions: hazard assessment using GIS and hydrological modeling. Mountain Research and Development 27: 336–344.

Benn DI, Wiseman S, Hands KA (2001) Growth and drainage of supraglacial lakes on debris-mantled Zgozumpa glacier, Khumbu Himal, Nepal. Journal of Glaciology 47(159): 626–639.

Bitelli G, Girelli VA (2009) Metrical use of declassified satellite imagery for an area of archaeological interest in Turkey. Journal of Cultural Heritage 10(S1): e25–e40.

Bolch T, Buchroither MF, Pieczonka T, Kunert A (2008a) Planimetric and volumetric glacier changes in the Khumbu Himal, Nepal, since 1962 using Corona, Landsat TM and ASTER data. Journal of Glaciology 54(187): 592–600.

Bolch T, Buchroithner MF, Peters J , Baessler M , Bajracharya SR (2008b) Identification of glacier motion and potentially dangerous glacier lakes at Mt. Everest area/Nepal using spaceborne imagery. Natural Hazards and Earth System Sciences 8: 1329-1340.

Byers A (2007) An assessment of contemporary glaciers fluctuations in Nepal's Khumbu Himal using repeat photography. Himalayan Journal of Sciences 4(6): 21–26.

Casana J, Cothren J (2008) Stereo analysis, DEM extraction and orthorectification of CORONA satellite imagery: archaeological applications from the Near East. Antiquity 82 (317): 732–749.

Dashora A, Lohani B, Malik JN (2007) A repository of earth resource information - CORONA satellite programme, Current Science 92: 926-932.

Fujii Y, Higuchi K (1977) Statistical analyses of the forms of the glaciers in Khumbu region. Journal of Japanese Society of Snow Ice (Special Issue) 39: 7–14.

Fujita K, Sakai A, Nuimura T, Yamaguchi S, Sharma RR (2009) Recent changes in Imja Glacial Lake and its damming moraine in the Nepal Himalaya revealed by in-situ surveys and multi-temporal ASTER imagery. Environmental Research Letters 4, 045205 (045207pp), doi:045210.041088/041748-049326/045204/045204/045205.

Fujita K, Suzuki R, Nuimura T, Sakai A (2008) Performance of ASTER and SRT DEMs, and their potential for assessing glacier lakes in the Lunana region, Bhutan Himalaya. Journal of Glaciology 54(185): 220–228.

Galiatsatos N, Donoghue DNM, Philip G (2008) High resolution elevation data derived from stereoscopic CORONA imagery with minimal ground control: an approach using Ikonos and SRTM data. Photogrammetric Engineering and Remote Sensing 74(9): 1093–1106.

Hambrey MJ, Quincey DJ, Glasser NF, Reynolds JM, Richardson SJ, Clemmens S (2008) Sedimentological, geomorphological and dynamic context of debris-mantled glaciers, Mountain Everest (Sagarmatha) region, Nepal. Quaternary Science Reviews 27: 2361–2389.

Hammond JE (1988) Glacial lakes in the Khumbu region, Nepal: An assessment of the hazards. MA Thesis, University of Colorado, Boulder, CO.

Ives JD, Shrestha RB, Mool PK (2010) Formation of Glacial Lakes in the Hindu Kush-Himalayas and GLOF Risk Assessment. ICIOMD.

Iwata S, Aoki T, Kadota T, Seko K, Yamaguchi S (2000) Morphological evolution of the debris-cover on Khumbu Glacier, Nepal, between 1978 and 1995. IAHS Publication No. 264: 3–11.

Kadota T, Seko K, Aoki T, Iwata S, Yamaguchi S (2000) Shrinkage of the Khumbu Glacier, east Nepal from 1978 to 1995. IAHS Publication No. 264: 235–243.

McDonald RA (1995) CORONA: Success for space reconnaissance. A look into the Cold War, and a revolution for intelligence. Photogrammetric Engineering and Remote Sensing 61: 689-720.

Mool PK, Bajracharya SR, Joshi SP (2001) Inventory of glaciers, glacial lakes and glacial lakes outburst floods, ICIMOD, Nepal.

Quincey DJ, Luckman A, Benn D (2009) Quantification of Everest region glacier velocities between 1992 and 2002, using satellite radar interferometry and feature tracking. Journal of Glaciology 55:596-606.

Quincey DJ, Richardson SD, Luckman A, Lucas RM, Reynolds JM, Hambrey MJ, Glasser NF (2007) Early recognition of glacial lake hazards in the Himalaya using remote sensing datasets. Global and Planetary Change 56(1–2): 137–152.

Reynolds MJ (2000) On the formation of supraglacial lakes on debris-covered glaciers. IAHS Publication No. 264 (Debris-covered Glaciers): 153–161.

Sakai A, Yamada T, Fujita K (2003) Volume change of Imja Glacier Lake in the Nepal Himalayas. International

Symposium on Disaster Mitigation and Basin Wide Water Management: 556–561.
Sakai A, Saito M, Nishimura K, Yamada T, Lizuka Y, Harada K, Kobayashi S, Fujita K, Gurung CB (2007) Topographical survey of end moraine and dead ice area at Imja glacier in 2001 and 2002. Bulletin of Glaciological Research 24: 29–36.
Slama C (1980) Manual of Photogrammetry, Fourth edition. The American Society for Photogrammetry and Remote Sensing, Falls Church.
Tadono T, Shimada M, Murakami H, Takaku J (2009) Calibration of PRISM and AVNIR-2 onboard ALOS "Daichi". Institute of Electrical and Electronics Engineers (IEEE) Transaction of Geoscience and Remote Sensing 47(12): 4042–4050.
Toutin T (2002) Three-dimensional topographic mapping with ASTER stereo data in rugged topography. Institute of Electrical and Electronics Engineers (IEEE) Transaction of Geoscience and Remote Sensing 40(10): 2241–2247.
Watanabe T, Ives JD, Hammond JE (1994) Rapid growth of a glacial lake in Khumbu Himal, Himalaya: prospects for a catastrophic flood. Mountain Research and Development 14(4): 329–340.
Watanabe T, Kameyama S, Sato T (1995) Imja glacier dead-ice melt rates and changes in a supra-glacial lake, 1989-1994, Khumbu Himal, Nepal: Danger of lake drainage. Mountain Research and Development 15(4): 293–300.
Watanabe T, Lamsal D, Ives JD (2009) Evaluating the growth characteristics of a glacial lake and its degree of danger of outburst flooding: Imja Glacier, Khumbu Himal, Nepal. Norsk Geografisk Tidsskrift 63(4): 255–267.
Yamada T (1998) Glacier lakes and its outburst flood in the Nepal Himalaya. Monograph No.1, Data Centre for Glacier Research, Japanese Society of Snow and Ice.
Ye Q, Zhong Z, Kang S, Alfred S, Wei Q, Liu J (2009) Monitoring Glacier and Supra-glacier Lakes from Space in Mt. Qomolngma Region of the Himalayas on the Tibetan Plateau in China. Journal of Mountain Science 6: 211-220.